Journal of Materials Chemistry A

Accepted Manuscript

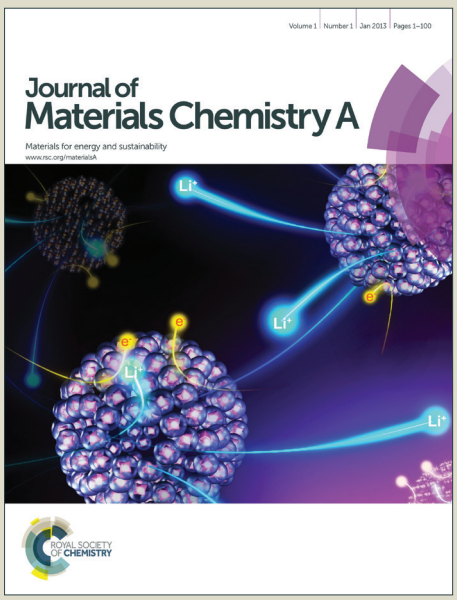

ROYAL SOCIETY OF CHEMISTRY

www.rsc.org/materialsA

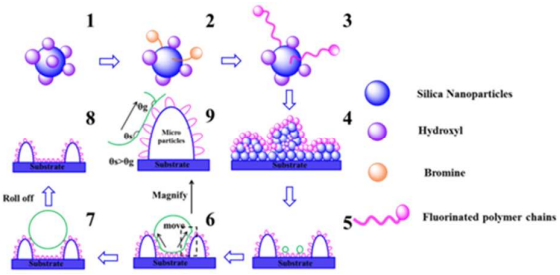

A novel anti-icing superhydrophobic hybrid material synthesized by Surface Initiated AGET ATPR can prevent ice formation thoroughly.

Journal of Materials Chemistry A

RSCPublishing

ARTICLE

A Novel Superhydrophobic Hybrid Nanocomposite Material Prepared by Surface-Initiated AGET ATRP and its Anti-icing Property

Cite this: DOI: 10.1039/x0xx00000x

Received ,
Accepted

DOI: 10.1039/x0xx00000x

www.rsc.org/

Xiaoli Zhan [§ a] *Yingdi Yan* [§ a] *Qinghua Zhang* [*a] *and Fengqiu Chen* [a]

Ice aggregation is a global challenge, especially for cold regions. In this article, a novel anti-icing hybrid material synthesized by grafting fluorinated polymer chains to silica nanoparticles via surface-initiated activators generated by electron transfer atom transfer radical polymerization (SI-AGET ATRP) was proposed. It showed such properties as controllable molecular design, wonderful thermal stability and high superhydrophobility. Most importantly, it exhibited excellent anti-icing property among coatings with different wettability varied from hydrophilic to superhydrophobic. Its large static water contact angle (WCA, 170.3°) and small contact angle hysteresis (CAH, <3°) can promote the removal of droplets efficiently. A new characterization method was put up to test the crystallization point of water, DSC, and its results demonstrated that the point can be depressed to a large extent (6.82°C). The low temperature WCA showed that it can postpone the freezing time from 196s to 10054s which indicates the surface can prevent ice formation thoroughly especially with the help of outside forces. The mechanisms were discussed based on physic-chemical property, heterogeneous nucleation theory and heat transfer theory. According to the present study, it is reasonable to predict that the organic-inorganic hybrid superhydrophobic coating will be prospective anti-icing candidate for various materials such as wind turbine blades, power lines and aircrafts.

Introduction

As we all know, ice adhesion and accumulation can lead to major inconvenience to individual daily life, such as traffic interruption, communicating destruction, loss of power and the damage of equipment relative to aviation, telecommunication, electricity and transportation.[1] In fact, it can also lead to major economic loss to countries. The snowstorms of southern China have caused huge economic losses up to several billions dollars during the Spring Festival of 2008. Thus, the research on anti-icing coatings is of great significance for the whole world. Nowadays, based on preventing ice formation and reducing ice adhesion strength, anti-icing coating and icephobic coating were brought up [2]. However, the anti-icing coating is better compared with the icephobic one for the latter one consumes energy more or less.

Preventing ice formation means retarding freezing time and reducing freezing temperature so that condensed water can roll off the substrates via outside power before it freezes, such as gravity, wind power and centrifugal forces. The classification of anti-icing coating can be described as hydrophilic, hydrophobic, and superhydrophobic. Spraying such chemicals as propylene glycol and ethylene glycol once used to delay crystallization because they can lower the freezing point of water. However, due to their hydrophility, the adhesion strength between water and substrate is large and it hinders the removal of condensed water. Then, hydrophobic coatings with low surface energy aroused interests because the large contact angle makes the rolling process easier. This kind of coatings mainly consists of fluorinated polymers [3, 4], organosilicone[5], fluoroalkylsilane[6, 7] and fatty acid[8]. Though it has the anti-icing effect, it is not ideal. In 1997, Barthlott et al.[9] revealed the famous lotus effect and then superhydrophobic materials began to be used as anti-icing coating and exhibited excellent performance thanks to their low surface energy and enhanced surface morphology. Up to now, it is still the research focus.[10-14]

Methods to create superhydrophobic surface are mainly attributed to two categories. One is mixing nanoparticles with low surface energy polymer physically [15]. However, for this kind of coating, it has been proved that after several ice/de-ice circles, the particle would shed off the surface [16, 17]because of the volume expansion during the process of icing or mechanical destruction during the process of de-icing, then the superhydrophobility was weakened. The other one is fabricated by chemical modification with low surface energy materials on textured surface [18-20]. To obtain surface with hierarchical roughness, pretreatment of substrates is necessary, such as chemical etching [21, 22], crystal growth [23, 24] and lithographic method [25, 26]. So, this method requires multi-steps and is not suitable to large area application.[27, 28] Taking these shortcomings into consideration, a coating which is

suitable for large area application and with excellent durability was synthesized by initiating polymerization from the surfaces of silica nanoparticles. Since the fluorinated polymer chains were grafted to particles, the covalent bond between surface and the polymer was strong enough to prevent separation. And the abrasive resistance was improved largely. Furthermore, the coating was very rigid. Though water expand while freezing, it is likely that the pressure created by trapped air lead to crack initiation and propagation as well as ice-bonding [29].

Besides, this kind of organic-inorganic hybrid material has other fascinating properties which cannot be obtained just by mixing inorganic nanoparticles with polymers. These composite materials conceive advantages of organic polymers and inorganic material. Organic parts provide controlled molecular structure and weight and good processability, while the inorganic parts offer high modulus, wonderful thermal and mechanical stability. Due to these remarkable physicochemical properties, organic-inorganic hybrid materials are applied in diverse fields such as nanomaterial, optoelectronic devices, catalysts, biology and so on [30-32]. However, their application in anti-icing field has few reports to the best of our knowledge.

It is widely known that grafting well-defined polymers on particles needs two steps. Firstly, introduce one or two initiators to the surface of particles and then grow polymer chains away from the interface gradually. This grafting-from approach can be carried out by living/controlled polymerizations [33-36], among which atom transfer radical polymerization (ATRP) is especially attractive for its tolerance of impurities, mild polymerization conditions and compatibility with a wide range of monomers. To overcome the drawbacks of normal ATRP such as challenging inert atmosphere, ATRP using activators generated by electron transfer (AGET) was developed [37, 38].

In this work, we synthesized a kind of organic-inorganic hybrid material by grafting poly (butylacrylate-*co*-2-(N-Ethylperfluorooctanesulphamido) acrylate) to silica nanoparticles via SI-AGET ATRP. By spin-coating the solution of this material, superhydrophobic surfaces were obtained. Its controllable polymerization, chemical composition and surface morphology were characterized by corresponding analysis methods. The anti-icing property was tested by, besides traditional contact angle hysteresis and water contact angle, differential scanning calorimetry (DSC) comparing with hydrophilic, hydrophobic and uncoated surfaces. Furthermore, the mechanisms were explored on the bases of physic-chemical property, heterogeneous nucleation theory and heat transfer theory.

Experimental

Materials

Fumed silica (SiO_2, >99.8%, 14nm) was purchased from Ximeng Chemical Co. 2-bromoisobutyryl bromide (BIBB, 98%), N,N,N',N'',N"-pentamethyldiethylenetriamine (PMDETA, 99%) and γ-aminopropyltriethoxysilane (APTES, >98%) were purchased from Aldrich Chemical Co. and used as received. Toluene was purchased from Sinopharm Chemical Reagent Co. and was purified by distillation from CaH_2. 2-(N-Ethylperfluorooctanesulphamido) acrylate (EFOA, >95%) was synthesized according to the literature [39]. and purified in acetone. Butyl methacrylate was purchased from Aldrich Chemical Co. and removed polymerization inhibitor by chromatography, then was stored in refrigerator under -4°C. Other reagents and organic solvents, unless specific illumination, were purchased from Sinopharm Chemical Regent Co. and used without any further purification.

Sample preparation

The approaches to prepare amino-functionalized, 2-bromoisobutyrate-functionalized and poly (BA-*co*-EFOA) grafted silica particles are shown in figure 1.

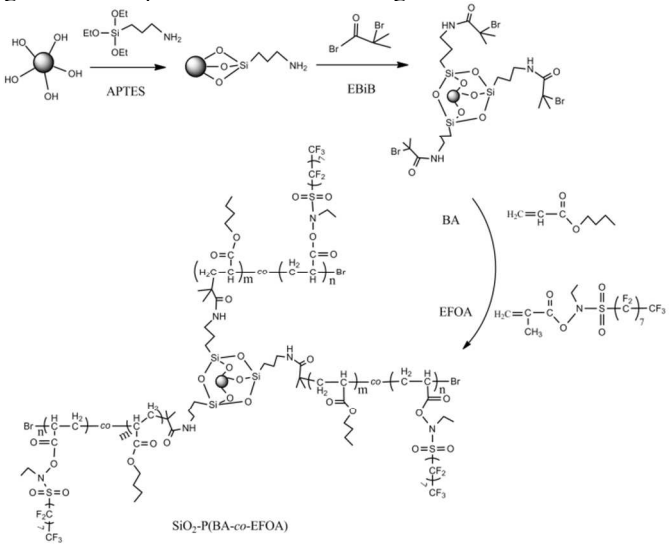

Fig.1 General approaches to prepare the amino-functionalized, 2-bromoisobutyrate-functionalized and poly (BA-*co*-EFOA) grafted silica particles

Synthesis of amino-functionalized silica nanoparticles SiO_2-NH_2 Typically, 15g of silica nanoparticles, 300 mL of anhydrous toluene and 21 mL of APTES were placed in a 500 mL round bottom flask equipped with a graham condenser. The reaction mixture was stirred by PTFE magnetic stir bar at 110°C under nitrogen atmosphere overnight and then cooled to ambient temperature. The nanoparticles were isolated by high-speed centrifugation and vacuum filtration. Then the sediments were redispersed in acetone and centrifuged again. The purification cycle mentioned above was repeated for several times to remove excess reagents. The product, named as SiO_2-NH_2, was dried in vacuum oven at 50°C for 6h.

Synthesis of amino-functionalized silica nanoparticles SiO_2-NH-Br 1.5g of SiO_2-NH_2 nanoparticles, 50 mL of dichloromethane and 0.5 mL of triethylamine were mixed in a round bottom flask immersed in an ice–water bath. After cooling to 0°C, the mixture of 2 mL of BiBB and 20 mL of dichloromethane were added dropwise. The solution was stirred at 0°C for 0.5 h and then at room temperature for 24 h. The method of isolation and purification of the product was similar to procedures described for SiO_2-NH_2. The final product, named as SiO_2-NH-Br was also dried under vacuum oven at 50 °C for 6h.

Synthesis of SiO_2-P(BA-*co*-EFOA) nano-composites via SI-AGET ATRP In this step, SiO_2-NH-Br (0.5g, 0.25mmol of initiating sites), BA (3.2g, 25mmol), EFOA (1.1g, 2.5mmol), PMDETA (0.05 mL, 0.25mmol), DMF solution of $CuBr_2$ (5%wt)

and anhydrous toluene (10mL) were added in a round bottom flask equipped with a magnetic stir bar. In order to make the SiO_2-NH-Br nanoparticles dispersed homogeneously, the mixture was treated by ultrasonication and then immersed in an ice-water bath. After purging the system with nitrogen for 20min, the toluene solution of $Sn(EH)_2$ (5%wt) (0.061g, 0.15mmol) was added through injection syringe . The flask was then transferred to an oil bath at 80°C. The ratio of BA: EFOA: CuBr: PMDETA: SiO_2-NH-Br was 100:10:1:1:1 in this study. After polymerization, the resulting solution was opened to air to terminate the polymerization, and then added into methanol and the nanoparticles were isolated via high-speed centrifugation. Redispersed in THF, the precipitation was isolated via centrifugation again. This purification cycle was repeated for three times. The final nanoparticles were dried at room temperature under vacuum overnight.

Spin Coating of SiO_2-P(BA-*co*-EFOA) nano-composites SiO_2-P(BA-*co*-EFOA) was dissolved in tetrahydrofuran (concentration 5wt%) and sonicated for 1 h prior use The solution was spin-coated onto clean glass slides at room temperature using a chemical technology KW-4A spinning coater. A rotational speed of 1200rpm and a holding time of 30s were chosen. After that the sample was allowed to evaporate slowly for a day. Then it was dried for 12h in a vacuum oven at 80°C and annealed at 130°C for 30 min.

Characterization

Characterization of controlled polymerization TGA was carried out on a TGA2050-TA Instrument (USA). The samples were analyzed under the nitrogen atmosphere with heating rate of 10°C/min from room temperature to 800°C. Molecular mass (Mn) and Molecular distributions (Mw/Mn) of the polymer were determined with GPC equipped with a Waters 1525 two-component high performance liquid chromatography pump, a Waters 717 automatic sampler, three Styragel HT columns and a Waters 2414 refractive index detector. A series of low-polydispersity polystyrene standards were employed for the GPC calibration. The eluent was tetrahydrofuran (THF) at 35°C with a flow rate of 1.0 mL/min. The polymer was cleaved from particles by hydrofluoric acid.

Characterization of superhydrophobic surfaces FTIR spectra were measured on Nicolet 5700 FT-IR spectrometer in the range of 4,000– 600cm−1. The samples were dissolved in THF and cast onto KBr disks to be analyzed. ^{1}H-NMR analysis was conducted with a Bruker 500 MHz nuclear magnetic resonance spectrometer (Advance DMX500) and was carried out with a 5wt% solution in $CDCl_3$ at room temperature, using tetramethylsilane (TMS) as internal reference. The chemical composition was analyzed by XPS (Thermo Scientific, USA) with an Al Kα X-ray source. The X-ray gun was operated at 14 kV and 350mW, and the analyzer chamber pressure was 10-9-10-10 Pa. The morphologies of the final particles were examined by TEM with a JEOL JEM-2010 transmission electron microscope (Tokyo, Japan). The solution was dipped onto carbon-coated copper grids and dried at room temperature. TEM was done at 80 kV. SEM analysis was performed using a JEOL SM 840 scanning electron microscope at an accelerating voltage of 20 kV. AFM was operated by Multi Mode (Veeco, USA) in tapping mode. The scanning range was 5μm × 5μm and the root-mean-square (RMS) roughness value was calculated from the obtained image.

Characterization of anti-icing properties A CAM 200 optical contact-angle goniometer (KSV Instruments, Helsinki, Finland) was used for CA measurements at both the ambient temperature and -18°C. The CAH was measured by tilting the sample stage from zero to higher angles until the droplet rolled off the surface, then the advanced angle and the receding angle can be calculated. The volume of the tested water droplet is 2μm.The influence on crystallization point of water was observed from the DSC with a DSC Q200 system (TA instruments). Before the DSC measurements, the sample pan was coated by the products with different wettability. The temperature ranges from room temperature to -50°C with a cooling rate of 10 °C/min.

Results and discussion

Figure 2 illustrated the whole process of preparation and application of superhydrophobic anti-icing surface. The pristine silica was functionalized by amino and 2-bromoisobutyrate, finally, poly (BA-*co*-EFOA) was grafted to functionalized silica particles. By spin-coating the solution of synthesized organic-inorganic hybrid material, we obtained micro-/nano-hierarchical structures due to surplus OH groups on silica nanoparticles facilitating moderate aggregation. Annealing process made fluorocarbon chains orientated to surface which, combined with roughness, lead to superhydrophobic surface. Just like lotus leaf [40], in humid environment, the micro water droplets are formed in on the valley. Then, converged microdroplets form a thin liquid layer on multipapillae. Due to the wettability gradient, the contact angle of upper edge (θg) is less than the lower one (θs). Driven by unbalanced surface tension, the microdroplet is deformed and directionally moves to top and finally, suspend on it. Since the adhesion between the droplet and surface is very low and both the crystallization point and time are changed to a large extent, the droplet can keep liquid for a long time and it can be removed by outside forces easily before it freezes. The detailed characterization concerning about controlled polymerization, chemical composition, surface morphology and anti-icing property are listed as follows.

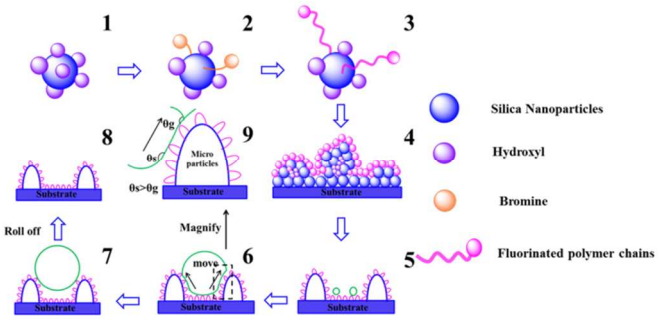

Fig.2 Schematic illustration of preparation and application of superhydrophobic anti-icing surface (1) Pristine silica nanoparticles (2) Fabrication of functionalized silica nanoparticles (3) Grafting fluorinated polymer chains to particles via SI-AGET ATRP (4) Formation of micro-/nano- hierarchical structures (5) Micro water droplets are formed in the valley (6) Converged microdroplets are deformed by unbalanced surface tension (7) Microdroplet directionally moves to top and finally, suspend on the surface (8) Water roll off with outside forces (9) Magnification of dashed frame illustrating the unbalanced surface tension caused by wettability gradient

Characterization of controlled polymerization

The TGA curves of pristine SiO_2, SiO_2-NH-Br and SiO_2-P(BA-*co*-EFOA) are shown in Figure 3(a). TGA has been proved to give good quantitative results relative to the Br content of the

samples in previous publications on similar systems because specific organic molecules pyrolyze at a specific temperature [41]. Using the assumption that under 200°C the weight loss was caused by the removal of water absorbed physically, the additional weight losses from SiO_2 and SiO_2-NH-Br were attributed to pyrolysis of hydroxyl and the introduced APTES respectively. On the basis of the data, it is feasible to quantify the yields of the synthesis using TGA. In order to circumvent any possible influence of physically absorbed water, the results were calculated by subtracting the weight loss under 200°C, 98.26% and 97.70% for SiO_2 and SiO_2-NH-Br respectively. With this method, the hydroxyl content of the SiO_2 is found to be 3.34mmol/g. From the TGA curve of SiO_2-NH-Br, the Br content of the SiO_2-NH-Br is found to be 0.495mmol/g, which determines the dosage of reagents used in the next step. As the TGA curve of SiO_2-P(BA-*co*-EFOA), besides the slight weight loss at about 200°C due to dehydration, the entire curve exhibits a large mass loss only between 300°C ~ 450°C, indicating that the polymer chain structure of the SiO_2 is homogeneous. To see whether the polymerization was living and controlled, the grafted polymers were cleaved from nanoparticles and GPC was tested. Its result was showed in Figure 3(b). We can clearly observe that there is a single peak curve and its PDI is 1.27. In other words, the characteristic of the resulting product is quite in line with AGET ATRP polymerization mechanism.

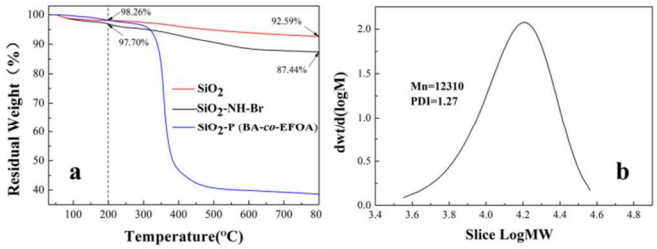

Fig.3 (a) TGA curves of the reference SiO_2, SiO_2-NH-Br and SiO_2-P(BA-*co*-EFOA) (b) GPC curve of grafted P(BA-*co*-EFOA)

Characterization of superhydrophobic surface

Superhydrophobic coatings are such coatings that are simultaneously characterized by a water contact angle greater than 150° and contact angle hysteresis smaller than 10°. The local contact angle, known as Young contact angle θ, can reach no more than 120° on planar surfaces even if the most efficient fluorine containing agents form a dense monolayer on the surface of texture elements [42]. By mimicking the natural superhydrophobic surfaces such as lotus leaves and insects' legs, superhydrophobic phenomenon are formed by combining surface chemical composition with surface roughness. As Figure 4 showed, two different models are proposed to explain this phenomenon: the Wenzel model [43] and the Cassie model [44]. Both of them displayed the real contact angle in function of the Young contact angle θ which was measured for a flat surface. The detailed information including equations and annotations for Young, Wenzel and Cassie model are displayed in Figure 4.

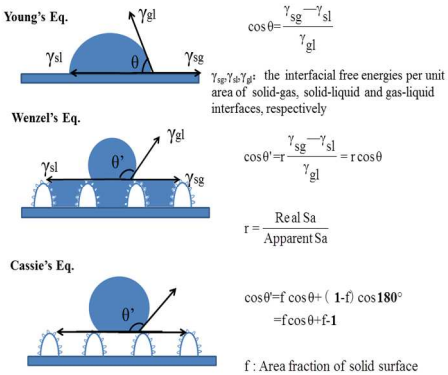

Fig.4 Young, Wenzel and Cassie's models

Characterization of chemical composition The chemical composition was tested by Fourier transform infrared (FT-IR), Nuclear magnetic resonance spectroscopy (^{1}H-NMR) and X-ray photoelectron spectroscopy (XPS).

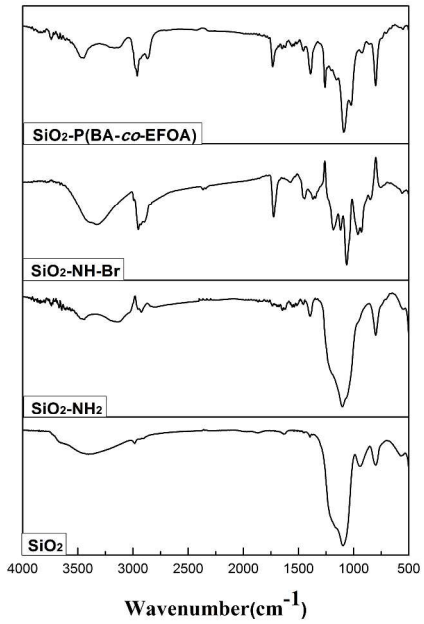

Fig.5 FT-IR spectrum of pristine SiO_2, SiO_2-NH_2, SiO_2-NH-Br and SiO_2-P（BA-*co*-EFOA）

The Figure 5 showed the FT-IR spectrometer of pristine SiO_2, SiO_2-NH_2, SiO_2-NH-Br and SiO_2-P (BA-*co*-EFOA). The broad absorption brands at about 1000-1250cm^{-1} corresponding to Si-O-Si stretching vibrations appeared in all of the SiO_2 related the samples. The brand observed at about 3446cm^{-1} indicated the presence of hydroxyl group in the surface of SiO_2 and the peak at 961cm^{-1} is attributed to Si-OH vibration. Compared with the FT-IR spectrum of pristine SiO_2, there was a -CH_2 stretching vibration at 2933cm^{-1}. The absence of Si-OH vibration at 961cm^{-1} showed hydroxyl group in the surface of silica was substituted. SiO_2-NH-Br macroinitiator was synthesized by the reaction of SiO_2-NH_2 with 2-bromoisobutyryl bromide. For SiO_2-NH-Br, C=O stretching vibrations of ester at 1629cm^{-1} occurs, which indicates the initiator group is linked. The FT-IR spectrum of SiO_2-P (BA-*co*-EFOA) showed the broad peak at 1100~1250cm^{-1} which is attributable to F-C-F stretching vibration. All of these proved that the graft polymerization via SI-AGET ATRP is successful.

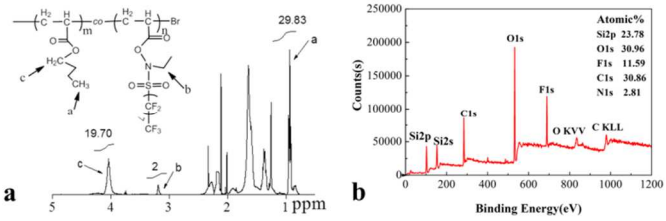

Fig. 6 (a) ^{1}H-NMR spectrum of cleaved polymer film (b) XPS survey spectrum of organic-inorganic hybrid silica particles

In Figure 6, the results of ^{1}H–NMR and XPS are showed together. We can infer the chemical composition of bulk and surface by analyzing them. Figure 6(a) showed the ^{1}H-NMR spectrum of cleaved polymer. As the figure shown, the H and its corresponding peak were annotated. According to the value of integrations, the ratio of m and n can be calculated as 10:1 which is in accordance with feed ratio. So the ratio of fluorine to carbon was obtained subsequently as 17:83 The overall XPS spectrum of the grafted silica nanoparticles' surface is depicted in figure 6 (b), and the silicon, oxygen, fluorine, carbon and nitrogen atomic percentage are estimated to be about 23.78%, 30.96%, 11.59%, 30.86% and 2.81% respectively. There is a high ratio of fluorine to carbon in the XPS data (11.59%: 30.86%=1: 2.66) than the realistic value of ^{1}H-NMR data (1:4.88), indicating that the fluorocarbon molecule chains migrated to the surface and this segregation makes the surface hydrophobic.

Characterization of surface morphology Transmission electron microscopy (TEM) photographs of primary silica nanoparticles and resultant organic-inorganic hybrid material are shown in Figure 7(a-c). In Figure 7(a), the aggregation can be observed clearly due to high specific surface area and high surface free energy of silica nanoparticles, as well as presence of OH groups on the nanoparticles surface. While in the Figure 7(c), polymers surrounding the silica can be seen obviously.[45] TEM micrographs of treated nanoparticles, Figure 7(b), showed that although grafted with polymers, the aggregation was slightly prevented. It is the key that why hierarchical surface morphology can form. Surplus OH groups facilitate aggregation but the polymer chains prevent it, the balance between the two contrary tendencies makes the treated particles form micro-nano particles with nano polymer hair among which fluorocarbon chains orientated to surface. These contribute to superhydrophobic property.

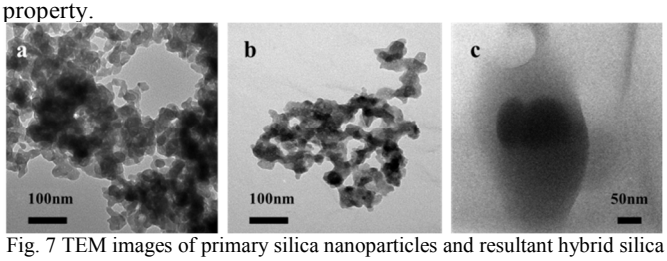

Fig. 7 TEM images of primary silica nanoparticles and resultant hybrid silica particles

According to figure 7, the particles assembled to form hierarchical roughness and make the surface superhydrophobic. The visible images of surface morphology are received by SEM and AFM. The corresponding images are showed in Figure 8. It is seen that the surface asperities are inhomogeneous. In the case of low magnification of SEM, the protuberances in micron scale are observed obviously. After magnifying, scattered nanoparticles can be seen as well, such as the area marked by red circle in figure 8(b). The surface topography obtained by the AFM images agrees pretty well with that from the SEM images. In addition, the micro/nano composite morphology of the surfaces obtained (AFM and SEM) perfectly matches the contact angle result which is showed in the top right corner of Figure 8(b), 170.3°.

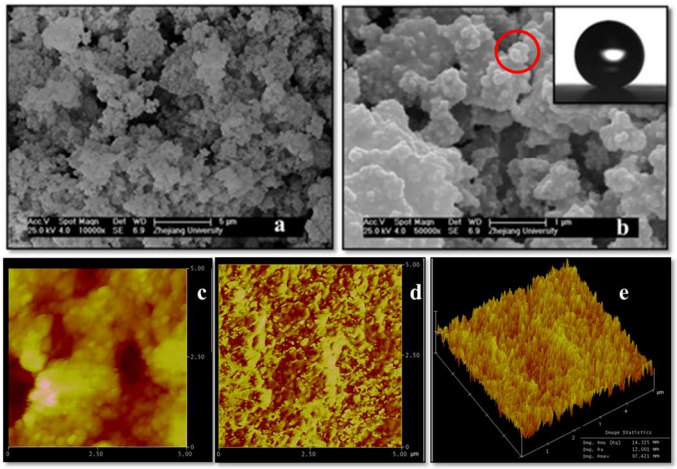

Fig.8 (a) SEM micrograph of the hybrid silica particles at 10000 times magnification (b) SEM micrograph of the hybrid silica particles at 50000 times magnification (c) AFM 2D height image of the hybrid silica particles (d) AFM 2D phase image of the hybrid silica particles (e) AFM 3D phase image of the hybrid silica particles

Through figure 8(d) and (e), we can obviously observe the scattered peaks on relatively flat the surface. That is why in figure 8(e), the RMS is 14.325nm while the Rmax is 97.421nm. The spacing between the textural peaks of the roughness is important for the trapping of air pockets [46]. Hence for the prepared hybrid material, the water droplet cannot penetrate the pitch profile which result in a high static contact angle and low adhesion.

Anti-icing property of superhydrophobic surface

Anti-icing property mainly refers to easy removal of condensed water before it freezes and delay in the crystallization of condensed water. So that ice accumulation can be prevented thoroughly. The anti-icing property is characterized by contact angle measurement in both ambient and subzero environment and DSC measurement. In this part, five samples with different wettability were used.

Removal of condensed water before crystallization The crucial factor determining whether it is easy for condensed water to roll off the surface is the force between condensed water and the surface. Lower force makes the removal procedure easier. As for superhydrophobic surface, the force is reduced by two methods, decreasing the contact area and reducing the contact angle hysteresis.

As we all know, large contact angle is echoed with small contact area. What's more, when the superhydrophobic surface is wetted by liquid, air is trapped inside the grooves in the hierarchical structure. So the real contact area refers to the fraction of the wetted area. It has been reported that the real contact area is generally considerably less than 10% for superhydrophobic surface due to the presence of an air layer [47]. Table 1 shows the contact angles of samples with different wettability. According to it, we can conclude that the

superhydrophobic surface decreased the contact area to a large extent.

In the case of contact angle hysteresis, it determines the force preventing the liquid rolling off the surface [48]. The lower the hysteresis, the more efficiently the drops are removed from a horizontal surface of a coating under a wind force or air stream pressure. The equation are showed in equation (1)

$$\Delta\theta = \theta_{adv} - \theta_{rec} \quad (1)$$

in which △θ, θadv and θrec represent the contact angle hysteresis, advancing contact angle and receding contact angle respectively. θ, θadv and θrec are marked in figure 9

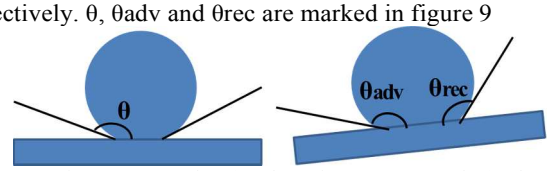

Fig.9 static contact angle (θ), advancing contact angle (θadv) and receding contact angle (θrec)

Table1 Contact angle (θ), advancing contact angle (θadv), receding contact angle (θrec) and contact angle hysteresis (△θ) for different surfaces achieved by CAM 200 optical contact-angle goniometer

	θ (°)	θadv (°)	θrec (°)	△θ (°)
A	51.5±0.5	63.7±2.1	34.7±1.7	29.9±1.2
B	40.3±0.7	73.6±1.6	22.7±1.6	50.9±0.2
C	103.0±0.2	116.9±1.8	68.6±2.1	48.3±3.9
D	113.5±0.1	129.8±1.2	99.8±1.8	29.8±2.0
E	170.3±2.4	171.5±2.1	168.7±1.9	2.7±0.2

Sample A, B, C D and E represent uncoated surface and the surface formed by pristine SiO_2, P (BA-*co*-EFOA), SiO_2-PBA and SiO_2-P (BA-*co*-EFOA) respectively. The proportion of BA and EFOA in C and E is equal.

According to the contact angle data, we can find that sample B, C, D and E exhibited hydrophility, double hydrophobicity and superhydrophobility respectively. Compared with hydrophilic, uncoated and hydrophobic surfaces, superhydrophobic surface reduced both the contact area and the force between water and surface to a large extent. We can conclude that the condensed water can roll off the surface as long as it is tilted slightly. On the other hand, to investigate the low adhesion between water and coating, we applied a super large droplet which is 7.5 times larger than normal one, 15μm. As Fig 10 showed, even if we pressed it hard, it is difficult for the droplet to paste on the surface. So, it is rational to say that the synthesized hybrid nanoparticles perceive good anti-icing property. Furthermore, it has been proved that the ice adhesion strength on rough hydrophobic surfaces has good correlation with wetting hysteresis.[49, 50]

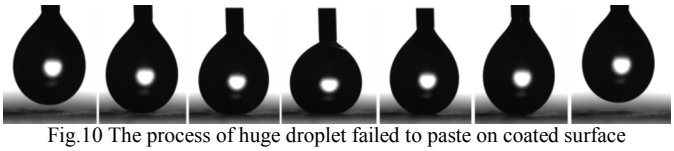

Fig.10 The process of huge droplet failed to paste on coated surface

Delay in the crystallization of condensed water The crystallization point of water droplet on surfaces with different coatings were obtained by DSC measurement at a continuously lowering temperature and the whole icing process of condensed water was observed by CAM 200 optical contact-angle goniometer at a constant temperature, -18°C.

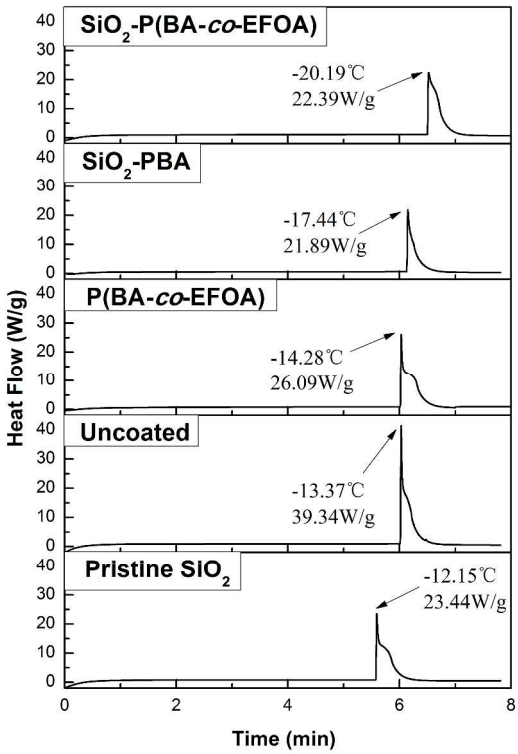

Fig.11 DSC curves of supercooled water droplets dripped into untreated crucible and crucible treated with pristine SiO_2, P (BA-*co*-EFOA), SiO_2-PBA and SiO_2- P (BA-*co*-EFOA). The temperature was set to decrease with the rate of 10°C/min

Through analyzing the DSC data, we can find that compared with the droplet dripped into untreated crucible, the one in hydrophilic, hydrophobic and superhydrophobic crucible possesses lower heat flow. It is clearly caused by the heat insulation of both coatings and trapped air between water and substrate. So, the reason why freezing point can be influenced is the key and needs to be discussed. The sample coated with pure polymer, P (BA-*co*-EFOA), is the only planar surface. The reduced crystallization temperature is attributed to adiabatic coating which actually influenced the temperature slightly. However, for other rough samples, this phenomenon can be explained by the combination of Kelvin's law and Clapeyron Relationship because numerous nanoparticles aggregated on the surface forming roughness especially for superhydrophobic surface, nano-hairs scattered on micron particles leading to capillaries. The formula of Kelvin's law is

$$Pr = \mathrm{P}\, exp(\frac{2\gamma V_m}{RTr}) \quad (2)$$

where Pr and P are the vapor pressure and saturated vapor pressure at a given temperature respectively; γ is the surface energy; V_m is the molar volume of phase; R is the gas constant; T is the temperature and r is the radius of little droplet or crystal. The value of r depends on the interface. If it is concave, r is positive and if it is convex, r is negative. So, it can be obviously observed that for hydrophilic surface (pristine SiO_2), Pr decreases while r decreases. While for SiO_2-PBA and SiO_2- P (BA-*co*-EFOA) coated surface, Pr increases when r decreases. Suspending on the surface with nano scales, r is little enough to generate a large Pr. Based on Clapeyron Relationship,

$$\frac{\mathrm{d}T}{\mathrm{d}p} = \frac{T\Delta_\alpha^\beta V_m}{\Delta_\alpha^\beta H_m} \quad (3)$$

where T is the temperature, p is the vapour pressure, $\Delta_{\alpha}^{\beta}Vm$ and $\Delta_{\alpha}^{\beta}Hm$ are volume difference and enthalpy change from phase α to β respectively. For solidification, the equation (3) transformed as

$$\frac{\mathrm{d}T}{T} = \frac{\Delta_{\mathrm{sol}} V_{\mathrm{m}}}{\Delta_{\mathrm{sol}} H_{\mathrm{m}}} \mathrm{d}\, p \tag{4}$$

After integral, we get

$$\ln \frac{T_2}{T_1} = \frac{\Delta_{\mathrm{sol}} V_{\mathrm{m}}}{\Delta_{\mathrm{sol}} H_{\mathrm{m}}} (p_2 - p_1) \tag{5}$$

Since in the process of solidification, $\Delta V_m>0$ and $\Delta H_m<0$, so, T is negatively related to P. Therefore, compared with uncoated surface, hydrophilic surface with certain roughness possess a lower pressure, so the water droplet on it solidified at a higher temperature (-12.15°C vs. -13.37°C) and water droplet on a hydrophobic surface with a higher pressure tends to be supercooled and the freeze temperature is correspondingly decreased (-17.44°C vs. -13.37°C). Thanks to its smaller r, the one on superhydrophobic surface was even lower (-20.19°C). While for the P (BA-*co*-EFOA) coated surface, the pressure is similar to smooth surface. This is why the temperature is in close proximity to the one on uncoated surface. According to the observation of DSC, we can conclude that the crystallization point of water can be reduced by optimizing the surface roughness and chemical composition. As for the superhydrophobic surface we applied, it decreased the temperature by 6.82°C. Besides decreasing crystallization point, the surface can delay crystallization compared with other surfaces at a constant temperature as well.

The photographs of individual water droplets on untreated glass and glass coated with different coatings in the whole freezing process are showed in figure 12. It can be obviously observed that the transparent center of condensed water vanished when the water began to freeze because the difference in reflectivity between water and ice [3]. The recorded data demonstrates that hydrophilic coating shortened the freezing process by 8s, planar and rough hydrophobic coating delayed it by 162s and 236s respectively, and most importantly, the superhydrophobic coating delayed it by 9858s which indicates this kind of coating can prevent ice formation thoroughly.

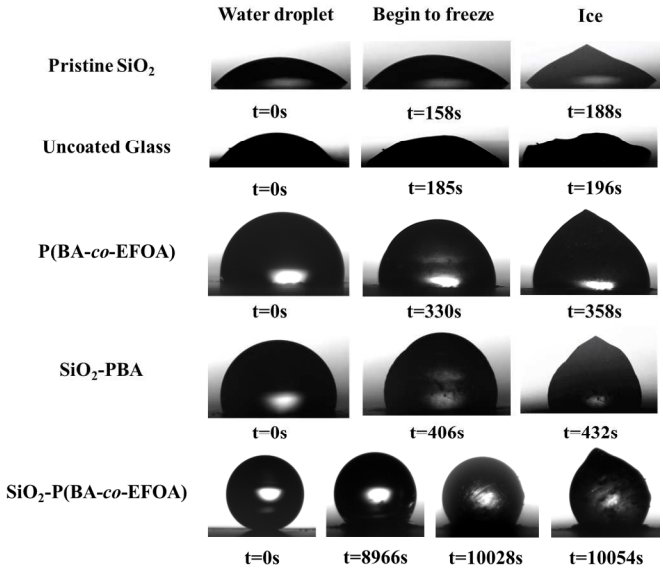

Fig.12 Photographs of individual water droplets on glasses with different coatings during the whole freezing process captured by a high speed CCD camera of CAM 200optical contact-angle goniometer

This phenomenon can be explained thermodynamically. It is well known that a water droplet must overcome the potential barrier to crystallize. For superhydrophobic surface, due to its roughness, the crystallization can be described as heterogeneous nucleation. Based on classic nucleation theory [51], the nucleation free energy barrier (ΔG) can be calculated by the equations

$$\Delta G = (\frac{2\pi R^3}{3}\Delta g + 2\pi R^2 \gamma_{sl}) f(\theta) \tag{6}$$

$$f(\theta) = \frac{(2 + \cos\theta)(1 - \cos\theta)^2}{4} \tag{7}$$

Where R is the droplet radius, γsl is the solid-liquid interfacial tension, Δg is the Gibb's energy density difference between ice and liquid water and θ is the apparent contact angle. According to the equations, ΔG is positively proportional to f(θ) which means that the bigger θ is, the higher ΔG is. The curve of f(θ) is shown in figure 13 from which we can see f(θ) is monotonously increasing with θ. So, the growing contact angle will enlarge the nucleation free energy barrier and retard the crystallization of condensed water. For treated glass with high superhydrophobility in this study, it is inevitable to delay the water droplet freeze.

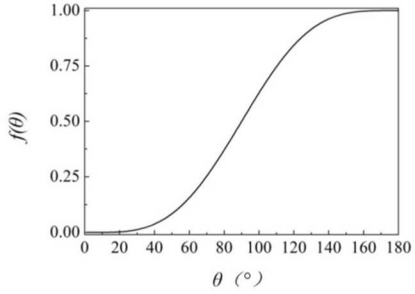

Fig. 13 The curve of f(θ) in the function of θ

Since trapped air existed between condensed water and cold superhydrophobic substrates, we believe that the droplet on surface is a system of three-phase interfaces. The process of heat transfer is changed correspondingly which also relative to the delay of crystallization. The heat transfer consists of the heat gains from air

via contact heat conduction and thermal radiation and the heat loss to nano polymer chains via the same way [24]. The equation of heat transfer is expressed as follows

$$Q = Q_{gc} + Q_{gr} - Q_{sc} - Q_{sr} \quad (8)$$

Where Q is the net heat gain in unit times, and Q >0 for a superhydrophobic surface at higher temperature; Q_{gc} and Q_{gr} are heat gains through heat conduction and thermal radiation in unit time; Q_{sc} and Q_{sr} are heat loss through heat conduction and thermal radiation in unit time. According to Fourier's law

$$Q_c = \int_{T_1}^{T_2} KSdT \quad (9)$$

Where Qc is heat transfer caused by conduction; K is the heat transfer coefficient, T_1 and T_2 are the temperatures of condensed water droplet and surface; S is the contact area. Thereby Qc is determined by S because K is the same for all surfaces. For the synthesized superhydrophobic coating, its nanohairs take up a tiny room and the trapped air took up very high percentage. All of these increase the heat gains and decrease the heat loss of heat conduction. Furthermore, the smaller liquid-solid contact area causes the loss of thermal radiation smaller. To sum up, superhydrophobic surface can gain much heat. According to the relationship between the decreased temperature (ΔT) in the droplet and net heat gain (Q)

$$\Delta T = \frac{\rho_w C_p (T_1 - T_2)}{Q} \quad (10)$$

where ρ_w is water density; Cp is the heat capacity of pure water at constant pressure. ΔT is negatively proportional to Q, that is to say a large Q can lead to a small ΔT. Thus it can explain why superhydrophobic surface can delay condensed water crystallization. Without the trapped air, the P (BA-*co*-EFOA) behaved worse than the SiO_2-PBA one although both of them are hydrophobic.

Conclusions

In this work, we proposed a novel anti-icing coating material with high superhydrophobility which was synthesized by grafting fluorinated polymer chains from the surface of silica nanoparticles via AGET ATRP and has not been made and investigated in previous studies. This material, compared with other reported ones, exhibited fascinating advantages such as high contact angle (170.3°) and abrasive resistance thanks to the inorganic part and the covalent bond between organic and inorganic materials. Its controllable polymerization, chemical composition and morphology were characterized by several methods and the results showed that a superhydrophobic coating was synthesized successfully and the process of polymerization was living and controllable. Most importantly, its anti-icing property was better than the ones reported previously. Our coating not only could promote the removal of droplets but also showed wonderful function on the aspect of lowering the crystallization point and delaying the freezing time. The crystallization temperature was reduced by 6.82°C and the water droplet on -18°C surface would not freeze until 10054s. What's more, the mechanisms of anti-icing property were discussed in details. Finally, based on present research, it is reasonable to predict that the organic-inorganic hybrid superhydrophobic coating will be prospective candidate for anti-icing material.

Acknowledgements

This work is continuously supported by the National Natural Science Foundation of China (Grant Nos. 21076184, 21176212 and 21276224)

Notes and references

[a] Department of Chemical and Biological Engineering, Zhejiang University, Hangzhou, 310027, China
§ These authors contributed equally

[1] Mishchenko L, Hatton B, Bahadur V, et al. Design of Ice-free Nanostructured Surfaces Based on Repulsion of Impacting Water Droplets[J]. ACS Nano. 2010, 4(12): 7699-7707.
[2] Yan Y D, Luo N Zh, Xiang X G, et al. Fabricating Mechanism and Preparation of Anti-icing & Icephobic Coating [J]. Prog. Chem. 2014, 26(01): 214-222.
[3] Li H, Zhao Y H, Yuan X Y. Facile preparation of superhydrophobic coating by spraying a fluorinated acrylic random copolymer micelle solution[J]. Soft Matter. 2013, 9(4): 1005-1009.
[4] Zou H L, Lin S D, Tu Y Y, et al. Simple approach towards fabrication of highly durable and robust superhydrophobic cotton fabric from functional diblock copolymer[J]. J. Mater. Chem. A. 2013, 1(37): 11246-11260.
[5] Park S H, Cho E H, Sohn J, et al. Design of multi-functional dual hole patterned carbon nanotube composites with superhydrophobicity and durability[J]. Nano Res. 2013, 6(6): 389-398.
[6] Boinovich L B, Emelyanenko A M, Ivanov V K, et al. Durable Icephobic Coating for Stainless Steel[J]. ACS Appl. Mater. Inter. 2013, 5(7): 2549-2554.
[7] He M, Zhang Q, Zeng X, et al. Hierarchical porous surface for efficiently controlling microdroplets' self-removal.[J]. Adv. Mater. 2013, 25(16).
[8] Koch K, Bhushan B, Jung Y C, et al. Fabrication of artificial Lotus leaves and significance of hierarchical structure for superhydrophobicity and low adhesion[J]. Soft Matter. 2009, 5(7): 1386-1393.
[9] Solga A, Cerman Z, Striffler B F, et al. The dream of staying clean: Lotus and biomimetic surfaces[J]. Bioinspir. Biomim. 2007, 2(4): S126-S134.
[10] Zhang Y L, Xia H, Kim E, et al. Recent developments in superhydrophobic surfaces with unique structural and functional properties[J]. Soft Matter. 2012, 8(44): 11217-11231.
[11] Rahmawan Y, Xu L B, Yang S. Self-assembly of nanostructures towards transparent, superhydrophobic surfaces[J]. J. Mater. Chem. A. 2013, 1(9): 2955-2969.
[12] Boreyko J B, Collier C P. Delayed Frost Growth on Jumping-Drop Superhydrophobic Surfaces[J]. ACS Nano. 2013, 7(2): 1618-1627.
[13] Wilson P W, Lu W Z, Xu H J, et al. Inhibition of ice nucleation by slippery liquid-infused porous surfaces (SLIPS)[J]. Phys Chem Chem Phys. 2013, 15(2): 581-585.
[14] Miljkovic N, Preston D J, Enright R, et al. Electrostatic charging of jumping droplets[J]. Nat. Commun. 2013, 4(2517).
[15] Sun W, Zhou S X, You B, et al. A facile method for the fabrication of superhydrophobic films with multiresponsive and reversibly tunable wettability[J]. J. Mater. Chem. A. 2013, 1(9): 3146-3154.
[16] Karmouch R, Ross G G. Experimental Study on the Evolution of Contact Angles with Temperature Near the Freezing Point[J]. J. Phys. Chem. C. 2010, 114(9): 4063-4066.
[17] Kulinich S A, Farhadi S, Nose K, et al. Superhydrophobic Surfaces: Are They Really Ice-Repellent?[J]. Langmuir. 2011, 27(1): 25-29.
[18] He M, Wang J J, Li H L, et al. Super-hydrophobic surfaces to condensed micro-droplets at temperatures below the freezing point retard ice/frost formation[J]. Soft Matter. 2011, 7(8): 3993-4000.
[19] Liu X J, Liang Y M, Zhou F, et al. Extreme wettability and tunable adhesion: biomimicking beyond nature?[J]. Soft Matter. 2012, 8(7): 2070-2086.
[20] Mishchenko L, Hatton B, Bahadur V, et al. Design of Ice-free Nanostructured Surfaces Based on Repulsion of Impacting Water Droplets[J]. ACS Nano. 2010, 4(12): 7699-7707.
[21] Ruan M, Li W, Wang B S, et al. Preparation and Anti-icing Behavior of Superhydrophobic Surfaces on Aluminum Alloy Substrates[J]. Langmuir. 2013, 29(27): 8482-8491.
[22] Wang Y Y, Xue J, Wang Q J, et al. Verification of Icephobic/Anti-icing Properties of a Superhydrophobic Surface[J]. ACS Appl. Mater. Inter. 2013,

5(8): 3370-3381.
[23] Li W, Zhang X, Yang J, et al. In situ growth of superbydrophobic and icephobic films with micro/nanoscale hierarchical structures on the aluminum substrate[J]. J. Colloid. Interf. Sci. 2013, 410: 165-171.
[24] Guo P, Zheng Y M, Wen M X, et al. Icephobic/Anti-Icing Properties of Micro/Nanostructured Surfaces[J]. Adv. Mater. 2012, 24(19): 2642-2648.
[25] Zhang Q, He M, Chen J, et al. Anti-icing surfaces based on enhanced self-propelled jumping of condensed water microdroplets.[J]. Chem. Commun. 2013, 49(40).
[26] Badge I, Bhawalkar S P, Jia L, et al. Tuning surface wettability using single layered and hierarchically ordered arrays of spherical colloidal particles[J]. Soft Matter. 2013, 9(11): 3032-3040.
[27] Brassard J, Sarkar D K, Perron J. Synthesis of Monodisperse Fluorinated Silica Nanoparticles and Their Superhydrophobic Thin Films[J]. ACS Appl. Mater. Inter. 2011, 3(9): 3583-3588.
[28] Du X, Li J, Li L, et al. Porous poly(2-octyl cyanoacrylate): a facile one-step preparation of superhydrophobic coatings on different substrates[J]. J. Mater. Chem. A. 2013, 1(4): 1026-1029.
[29] Menini R, Farzaneh M. Advanced Icephobic Coatings[J]. J. Adhes. Sci. Technol. 2011, 25(9): 971-992.
[30] Sanchez C, Belleville P, Popall M, et al. Applications of advanced hybrid organic-inorganic nanomaterials: from laboratory to market[J]. Chem. Soc. Rev. 2011, 40(2): 696-753.
[31] Yuan K, Chen L, Li F, et al. Nanostructured hybrid ZnO@ CdS nanowalls grown in situ for inverted polymer solar cells[J]. J. Mater. Chem. C. 2014.
[32] Yu H J, Luo Z H. Novel superhydrophobic silica/poly (siloxane‐fluoroacrylate) hybrid nanoparticles prepared via two‐step surface‐initiated ATRP: Synthesis, characterization, and wettability[J]. J. Polym. Sci. Part A: Polym. Chem. 2010, 48(23): 5570-5580.
[33] Fu R, Fu G. Polymeric nanomaterials from combined click chemistry and controlled radical polymerization[J]. Polym. Chem. 2011, 2(3): 465-475.
[34] Kakwere H, Perrier S. Design of complex polymeric architectures and nanostructured materials/hybrids by living radical polymerization of hydroxylated monomers[J]. Polym. Chem. 2011, 2(2): 270-288.
[35] Liu J, Ma S, Wei Q, et al. Parallel array of nanochannels grafted with polymer-brushes-stabilized Au nanoparticles for flow-through catalysis[J]. Nanoscale. 2013, 5(23): 11894-11901.
[36] Moraes J, Ohno K, Maschmeyer T, et al. Synthesis of silica–polymer core–shell nanoparticles by reversible addition–fragmentation chain transfer polymerization[J]. Chem. Commun. 2013, 49(80): 9077-9088.
[37] Min K, Gao H F, Matyjaszewski K. Preparation of homopolymers and block copolymers in miniemulsion by ATRP using activators generated by electron transfer (AGET)[J]. J. Am. Chem. Soc. 2005, 127(11): 3825-3830.
[38] Jakubowski W, Matyjaszewski K. Activator generated by electron transfer for atom transfer radical polymerization[J]. Macromolecules. 2005, 38(10): 4139-4146.
[39] Wang Q Y, Zhang Q H, Zhan X L, et al. Structure and Surface Properties of Polyacrylates with Short Fluorocarbon Side Chain: Role of the Main Chain and Spacer Group[J]. J. Polym. Sci. Part A: Polym. Chem. 2010, 48(12): 2584-2593.
[40] Zheng Y M, Han D, Zhai J, et al. In situ investigation on dynamic suspending of microdroplet on lotus leaf and gradient of wettable micro- and nanostructure from water condensation[J]. Appl. Phys. Lett. 2008, 92(0841068).
[41] Nielsen R, Kingshott P, Uyar T, et al. Characterization of beta-cyclodextrin modified SiO2[J]. Surf. Interface Anal. 2011, 43(5): 884-892.
[42] Jindasuwan S, Nimittrakoolchai O, Sujaridworakun P, et al. Surface characteristics of water-repellent polyelectrolyte multilayer films containing various silica contents[J]. Thin Solid Films. 2009, 517(17): 5001-5005.
[43] Wenzel R N. Resistance of solid surfaces to wetting by water[J]. Ind. Eng. Chem. 1936, 28: 988-994.
[44] Cassie A, Baxter S. Wettability of porous surfaces.[J]. Transactions of the Fadaday Society. 1944, 40: 546-550.
[45] Lee S G, Ham D S, Lee D Y, et al. Transparent Superhydrophobic/Translucent Superamphiphobic Coatings Based on Silica-Fluoropolymer Hybrid Nanoparticles[J]. Langmuir. 2013, 29(48): 15051-15057.
[46] Facio D S, Mosquera M J. Simple Strategy for Producing Superhydrophobic Nanocomposite Coatings In Situ on a Building Substrate[J]. ACS Appl. Mater. Inter. 2013, 5(15): 7517-7526.
[47] Boinovich L B, Emelyanenko A M. Anti-icing potential of superhydrophobic coatings[J]. Mendeleev. Commun. 2013, 23(1): 3-10.
[48] Kim P, Wong T S, Alvarenga J, et al. Liquid-Infused Nanostructured Surfaces with Extreme Anti-Ice and Anti-Frost Performance[J]. ACS Nano. 2012, 6(8): 6569-6577.
[49] Kulinich S A, Farzaneh M. How Wetting Hysteresis Influences Ice Adhesion Strength on Superhydrophobic Surfaces[J]. Langmuir. 2009, 25(16): 8854-8856.
[50] Meuler A J, Smith J D, Varanasi K K, et al. Relationships between Water Wettability and Ice Adhesion[J]. ACS Appl. Mater. Inter. 2010, 2(11): 3100-3110.
[51] Varanasi K K, Hsu M, Bhate N, et al. Spatial control in the heterogeneous nucleation of water[J]. Appl. Phys. Lett. 2009, 95(0941019).